mathematics

MDPI

Article

Fully Nonlinear Evolution of Free-Surface Waves with Constant Vorticity under Horizontal Electric Fields

M. V. Flamarion [1], E. Kochurin [2,3,*] and R. Ribeiro-Jr [4]

[1] Unidade Acadêmica do Cabo de Santo Agostinho, UFRPE/Rural Federal University of Pernambuco, BR 101 Sul, Cabo de Santo Agostinho 54503-900, PE, Brazil; marcelo.flamarion@ufrpe.br
[2] Institute of Electrophysics, Ural Branch of Russian Academy of Sciences, Yekaterinburg 620016, Russia
[3] Skolkovo Institute of Science and Technology, Moscow 121205, Russia
[4] Departamento de Matemática, Centro Politécnico, UFPR/Federal University of Paraná, Jardim das Américas, Caixa Postal 19081, Curitiba 81531-980, PR, Brazil; robertoribeiro@ufpr.br
* Correspondence: kochurin@iep.uran.ru

Abstract: This work presents the results of a direct numerical simulation of the nonlinear free surface evolution of a finite-depth fluid with a linear shear flow under the action of horizontal electric fields. The method of time-dependent conformal transformation for the description of the combined effects of the electric fields and constant vorticity is generalized for the first time. The simulation results show that strong shear flow co-directed in the wave propagation direction leads to the formation of large-amplitude surface waves, and, for some limiting vorticity value, a wave breaking process with the formation of an air bubble in the liquid is possible. The oppositely directed shear flow can cause the retrograde motion of a surface wave (wave propagation in the opposite direction to the linear wave speed). The simulations conducted taking into account the electro-hydrodynamic effects demonstrate that a high enough external horizontal electric field suppresses these strongly nonlinear processes, and the surface waves tend to preserve their shape.

Keywords: shear flow; conformal transformation; nonlinear waves; free surface; electric field; direct numerical simulation

MSC: 37M05

check for updates

Citation: Flamarion, M.V.; Kochurin, E.; Ribeiro-Jr, R. Fully Nonlinear Evolution of Free-Surface Waves with Constant Vorticity under Horizontal Electric Fields. *Mathematics* **2023**, *11*, 4467. https://doi.org/10.3390/math11214467

Academic Editor: Marco Pedroni

Received: 9 October 2023
Revised: 25 October 2023
Accepted: 26 October 2023
Published: 28 October 2023

Copyright: © 2023 by the authors. Licensee MDPI, Basel, Switzerland. This article is an open access article distributed under the terms and conditions of the Creative Commons Attribution (CC BY) license (https://creativecommons.org/licenses/by/4.0/).

1. Introduction

The problem of describing the interfacial electro-hydrodynamic motion of liquids is of great interest for many areas of modern physics and technology (see the review in [1] and references therein). Melcher showed [2] that an external electric field directed normal to the surface of a nonconducting liquid causes its instability, while a tangential electric field, on the contrary, has a stabilizing effect. The practical interest in studying the electro-hydrodynamics of the surface of liquids is determined by the possibility of controlling and stabilizing hydrodynamic instabilities [3–6]. Zubarev showed [7–10] that in the limits of a strong electric field, when the effects of gravity and capillarity are infinitesimal, the nonlinear dynamics of liquid boundaries can be effectively described analytically. In particular, it was shown that strongly nonlinear waves of an arbitrary shape can propagate without distortions at the surface of a liquid with a high dielectric constant under the action of a horizontal field. The Zubarev solution for surface electro-hydrodynamic waves is a complete analog of Alfv́en waves in plasmas, which play an important role in the development of magneto-hydrodynamic (MHD) turbulence [11]. Free-surface magnetic (or electric) wave turbulence as an analog to classic MHD turbulence was studied experimentally and theoretically in [12–14] and [15–17], respectively.

Until recently, the nonlinear dynamics of surface waves were considered only in the approximation of irrotational fluid flow (see, for instance, [18–20]). Great success in the

study of nonlinear waves on the surface of a liquid in the presence of a linear shear flow (constant vorticity) was achieved in [21–27]. These works did not consider the effects of external electric or magnetic fields. The electro-hydrodynamic motion of liquids in the presence of linear shear flow is still a poorly studied problem. The studies in [28,29] investigated the dynamics of water waves with constant vorticity under the action of only vertical electric fields. This work is focused on studying the combined influence of an external horizontal electric field and linear shear fluid flow on the dynamics of surface gravity–capillary waves. The analysis is based on the method of time-dependent conformal transformation, in which the area occupied by the liquid is transformed into a strip of canonical variables (see [30–32]). The principal advantage of the method is reducing the original spatially two-dimensional problem to a 1D equation system directly describing the motion of the fluid boundary. The conformal transformation method has proved to be very convenient for describing nonlinear waves at the free boundaries of liquids see [33–38]. The method was numerically generalized for the description of the electro-hydrodynamic motion of liquids with a free surface for horizontal and vertical fields in [39] and [40–43], respectively. To date, the method of dynamic conformal transformation has not yet been used for the description of free-surface waves with constant vorticity and an external horizontal electric field.

In this work, a series of numerical simulations of free-surface waves with constant vorticity under horizontal electric fields and a wide range of control parameters is presented the first time. As an initial condition, the work considers the evolution of a simple periodic wave, the deformation of which occurs only due to nonlinear effects. In the regime of strong vorticity, complex phenomena such as the wave breaking with the formation of a bubble in the liquid, as well as the retrograde propagation of a wave, when the shear flow is directed against the direction of the wave motion are observed for the first time.

2. Mathematical Formulation

2.1. Dynamic Equations

The dynamics of an inviscid and incompressible dielectric liquid (i.e., there are no electric charges inside the fluid) with a density ρ, mean depth h, and relative electric permittivity ϵ in a two-dimensional space $\{x, y\}$ are examined in the current work. The fluid is under the influence of an external horizontal electric field with a value of $E_0 = V_0/L$, where L is the horizontal size of the system, and V_0 is the potential difference along the horizontal axis. In the electrostatic limit of Maxwell's equations, the induced magnetic fields are negligible, thus resulting in an irrotational electric field due to Faraday's law. A potential function $V(x, y)$ of the electric fields $\vec{E}$ is introduced in such a way that $\vec{E} = -\nabla V$, and hence V satisfies the Laplace equation in the dielectric fluid layer. A schematic of the problem is presented in Figure 1. The surface tension coefficient is denoted by T. Let us introduce a Cartesian coordinate system $\{x, y\}$ with gravity pointing in the negative y-direction and $y = 0$ being the undisturbed free surface. In the unperturbed state, the potential of the electric field has the form of a linear function $V(x, y) = -(V_0/L)x$. The bottom boundary of the fluid is at $y = -h$, and the upper boundary is free to move and is denoted by $\eta(x, t)$.

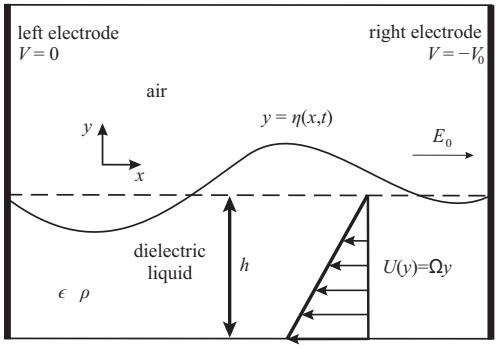


Figure 1. The geometry of the problem.

The present study assumes that flow in the dielectric fluid is rotational with constant vorticity Ω. In the unperturbed state, the velocity field in the fluid body is given by

$$\vec{U}_0 = (\Omega y, 0).$$

The background flow $\vec{U}_0$ is a linear shear flow with a horizontal velocity equal to zero at the free surface. For a positive Ω, the shear flow is directed opposite to the x-axis, and in the case of $\Omega < 0$, the direction of the shear flow is aligned with the horizontal axis. We consider the velocity field as

$$\vec{U} = \vec{U}_0 + \nabla\phi, \tag{1}$$

where ϕ is a velocity potential. Thus, the velocity constitutes an irrotational perturbation of the shear flow.

The dynamic equation system reads as:

$$\nabla^2\phi = 0 \qquad \text{in} - h < y < \eta(x,t), \tag{2}$$

$$\nabla^2 V = 0 \qquad \text{in} - h < y < \eta(x,t), \tag{3}$$

$$\eta_t + (\phi_x + \Omega\eta)\eta_x = \phi_y \qquad \text{for} \quad y = \eta(x,t), \tag{4}$$

$$\phi_y = 0 \qquad \text{for} \quad y = -h, \tag{5}$$

$$\partial V/\partial n = 0 \qquad \text{for} \quad y = \eta(x,t), \tag{6}$$

$$V_y = 0 \qquad \text{for} \quad y = -h, \tag{7}$$

where $\partial/\partial n$ stands for the normal derivative to a free surface. The expressions (6) and (7) come from the standard Maxwell's boundary conditions at the interface between dielectric media under the assumption $\epsilon \gg 1$. Zubarev [7,8] showed that, for the case of a liquid with a high dielectric constant, the electric field lines are directed tangentially to the free surface of the liquid, i.e., the field is tangential. In this case, the electrostatic problem can be completely solved using the method of conformal transformation, which will be discussed later in this work. The equation system (2)–(7) is supplemented by the dynamic boundary condition (Bernoulli equation):

$$\phi_t + \frac{1}{2}(\phi_x^2 + \phi_y^2) + \Omega\eta\phi_x - \Omega\psi = -g\eta + \frac{T}{\rho}\frac{\eta_{xx}}{(1+\eta_x^2)^{3/2}} + \frac{\epsilon_0\epsilon}{2\rho}|\nabla V|^2 + B, \tag{8}$$

where g is the gravity acceleration, ϵ_0 is the vacuum permittivity, and B is the Bernoulli constant. It should be mentioned that the Bernoulli dynamic boundary condition (8) can be used because the flow is laminar.

The above equation system describes the fully nonlinear evolution of a finite-depth dielectric liquid subjected to a tangential electric field taking into account the effects of gravity, surface tension, and constant vorticity. It is convenient now to introduce dimensionless notation by choosing the following quantities as characteristic values of the length, time, velocity potential, and electric field potential:

$$\left[\frac{T}{\rho g}\right]^{1/2}, \qquad \left[\frac{T}{\rho g^3}\right]^{1/4}, \qquad \left[\frac{T^3}{\rho^3 g}\right]^{1/4}, \qquad \frac{V_0}{L}\left[\frac{T}{\rho g}\right]^{1/2}.$$

In dimensionless form, the Bernoulli Equation (8) is rewritten as

$$\phi_t + \frac{1}{2}(\phi_x^2 + \phi_y^2) + \Omega\eta\phi_x - \Omega\psi = -\eta + \frac{\eta_{xx}}{(1+\eta_x^2)^{3/2}} + \frac{E_b}{2}|\nabla V|^2 + B, \tag{9}$$

where E_b is the nondimensional parameter characterizing the electric field

$$E_b = \frac{\epsilon_0\epsilon V_0^2}{L^2\sqrt{\rho g T}}.$$

It should be noted the quantity Ω in (9) is nondimensional, i.e., the vorticity is measured in units $\left[T/\rho g^3\right]^{-1/4}$, [s^{-1}].

2.2. Equations in Conformal Variables

The current study is based on the method of conformal transformation, in which the area occupied by the liquid is transformed into a canonical area in the form of a horizontal strip of uniform thickness denoted as D. The new independent conformal coordinates are $\{\xi, \zeta\}$. With such a transformation, the problem of velocity potential distribution is solved analytically, but the coordinate transformation remains unknown: $x = X(\xi, \zeta)$, $y = Y(\xi, \zeta)$. The functions $X(\xi, \zeta)$ and $Y(\xi, \zeta)$ are assumed to be harmonic; as a consequence, they can be represented as

$$Y(\xi, \zeta) = \mathbf{F}^{-1}\left[\frac{\sinh(k_j(\zeta + D))}{\sinh(k_j D)}\mathbf{F}_{k_j}[Y]\right] + \frac{\zeta}{D}, \tag{10}$$

and

$$X(\xi, \zeta) = \xi - \mathbf{F}^{-1}\left[i\frac{\cosh(k_j(\zeta + D))}{\sinh(k_j D)}\mathbf{F}_{k_j}[Y]\right], \quad j \neq 0 \tag{11}$$

where $k_j = 2\pi j L$ for $j \in \mathbb{Z}$, and

$$\mathbf{F}_{k_j}[g(\xi)] = \hat{g}(k_j) = \frac{1}{L}\int_{-L/2}^{L/2} g(\xi)e^{-ik_j\xi}\, d\xi,$$

$$\mathbf{F}^{-1}\left[\{\hat{g}(k_j)\}_{j\in\mathbf{Z}}\right] = \sum_{j=-\infty}^{+\infty} \hat{g}(k_j)e^{ik_j\xi}.$$

The free-surface profile corresponds to the $\zeta = 0$ line. Based on this fact and the expressions (10) and (11), we obtain the relation between $X(\xi, 0)$ and $Y(\xi, 0)$:

$$X(\xi) = \xi - \mathcal{T}[Y(\xi)],$$

with $\mathcal{T}[\cdot] := \mathbf{F}^{-1}\left[i\coth(k_j D)\mathbf{F}_{k_j}[\cdot]\right]$. In the context of this study, the computational domain is represented by $[-L/2, L/2)$, and L is selected to ensure that the wavelength in both the physical and canonical domains is identical. Hence, the following relation is satisfied:

$$D = \langle Y \rangle + h,$$

where

$$\langle Y \rangle = \frac{1}{L}\int_{-L/2}^{L/2} Y(\xi)\, d\xi.$$

The procedure for deriving the equations of motion in conformal variables is well known (see [22,30–32]). For this reason, we will simply present them, paying particular attention to the electric field term. To clarify the term responsible for the effect of electrostatic pressure, we introduce the perturbation of the electric field potential as $v = V + X$. Let the quantity θ be canonically conjugated to v (the electric analog to the fluid stream function ψ). From the Cauchy–Riemann conditions, one can obtain the relation between the potentials and the stream functions:

$$\phi_\xi = -\mathcal{T}[\psi_\xi], \qquad v_\xi = -\mathcal{T}[\theta_\xi]. \tag{12}$$

The physical interpretation of the condition (6) is that the electric field lines are directed tangentially to the free surface. This means that the function θ is completely determined by the geometry of the surface profile, namely,

$$\theta(\xi,\zeta) = Y(\xi,\zeta). \tag{13}$$

The expression (13) gives a complete solution of the electrostatic problem. From (13) and (12), it follows that the electric field potential is

$$V(\xi,\zeta) \equiv -\xi + \text{const}, \tag{14}$$

where the constant is found from the boundary conditions at $X = -L/2$ and $X = L/2$ to be $-L/2$. Thus, in conformal variables, the electric field potential V coincides up to a sign with the variable ξ. Using Green's theorem, we can write the electric field potential energy as

$$\frac{E_b}{2}\int\limits_{y<\eta}(\nabla V)^2 dxdy = \frac{E_b}{2}\int\limits_{-L/2}^{L/2}\theta v_\xi d\xi = -\frac{E_b}{2}\int\limits_{-L/2}^{L/2} Y\mathcal{T}[Y_\xi]d\xi.$$

The total energy of the system (Hamiltonian) has the form

$$H = \frac{1}{2}\int\limits_{-L/2}^{L/2}\left[\frac{1}{3}\Omega^2 Y^3 X_\xi + \Omega Y^2\phi_\xi - \phi\psi_\xi + Y^2 X_\xi + 2(J^{1/2} - X_\xi) - E_b Y\mathcal{T}[Y_\xi]\right]d\xi, \tag{15}$$

where $J = X_\xi^2 + Y_\xi^2$ is the Jacobian of the transformation. The equations of fluid motion are reduced to the pair of equations directly describing the dynamics of the boundary

$$Y_t = Y_\xi\mathcal{T}\left[\frac{\Psi_\xi}{J}\right] - X_\xi\frac{\Psi_\xi}{J}, \tag{16}$$

$$\phi_t = -Y - \frac{1}{2J}(\phi_\xi^2 - \psi_\xi^2) + \phi_\xi\mathcal{T}\left[\frac{\Psi_\xi}{J}\right] - \frac{1}{J}\Omega Y X_\xi\phi_\xi + \Omega\psi + \frac{X_\xi Y_{\xi\xi} - Y_\xi X_{\xi\xi}}{J^{3/2}} + \frac{E_b}{2J} + B, \tag{17}$$

where $\Psi_\xi = \psi_\xi + \Omega Y Y_\xi$. The system of Equations (16) and (17) describes the fully nonlinear evolution of the fluid surface taking into account gravity, surface tension, constant vorticity, and a tangential electric field. It should be noted that the system is very close to one describing the effect of a normal (vertical) field. In such a case, the electric field parameter is replaced by $E_b = -\epsilon_0\epsilon V_0^2/h^2\sqrt{\rho g T}$, and instead of the relation (14), we have $V(\xi,\zeta) \equiv -\zeta/D$ (see [41]). The factor $1/D$ arises to fulfil the boundary condition for the electric potential at the bottom. In the case of a tangential field, the factor $1/D^2$ is absent in the electric term in (17) as the wave period is the same in both the physical and conformal variables.

In the linear approximation, the equation system describes the propagation of surface waves with the speed

$$c_0 = -\frac{\Omega\tanh(kh)}{2k} \pm \left[\tanh(kh)\left(\frac{1}{k} + k\right) + E_b + \left(\frac{\Omega\tanh(kh)}{2k}\right)^2\right]^{1/2}, \tag{18}$$

where signs $\pm$ correspond to the direction along which the wave travels (along or against the direction of the x-axis). From the expression (18), it follows that positive vorticity slows down the wave propagating to the positive direction of the x-axis. The negative vorticity, on the contrary, accelerates the wave propagation. In the case of a strong electric field,

$$E_b \gg \tanh(kh)\left(\frac{1}{k} + k\right) + \left(\frac{\Omega\tanh(kh)}{2k}\right)^2, \tag{19}$$

the system of Equations (16) and (17) has an exact analytical solution in the form of a nonlinear wave of arbitrary shape traveling with the velocity $V_A = E_b^{1/2}$ (an analog to the Alfvén speed) along or against the x-axis (for more details, see [7,8]). From this solution, one can find the Bernoulli constant $B = -E_b/2$.

3. Results

The numerical solution of Equations (16) and (17) is based on the standard pseudo-spectral methods for the calculation of spatial derivatives and integral operators. As a consequence, the boundary conditions are periodic in space. The total number of Fourier harmonics is equal to $N = 2048$. To suppress the aliasing effect, we used a filter that nulled higher harmonics with a wavenumber above $k_a \geq N/3$. All calculations were carried out in a periodic region of the length $L = 2\pi$. Integration over time was carried out using the explicit Runge–Kutta method of fourth-order accuracy with the step dt. The time step was comparable to the period of the fastest surface wave, i.e., $dt \leq 2\pi/\max(c_0 k)$. This condition was satisfied for the time step of the value $dt = 0.5 \cdot 10^{-4}$. The parameter $D(t)$ was calculated using the iteration method from the law of mass conservation. The iterations were stopped when the relative error in estimating the mass of the liquid reached a small value of 10^{-10}.

The initial conditions were taken in such a way that in the linear approximation they describe the propagation of a simple periodic wave with a constant velocity. The corresponding initial condition for the function Y is the following:

$$Y(\xi, 0) = A \cdot \cos(X(\xi, 0)), \qquad t = 0, \tag{20}$$

where A is the wave amplitude. It is should be noted that the initial condition (20) is specified explicitly through the function $X(\xi)$. In order to express the dependence $Y = Y(\xi)$, we used the iterative method of successive approximations:

$$Y_i = A\cos(X_i), \qquad X_i = \xi - \mathcal{T}[Y_i],$$

with the initial approximation $Y_1(\xi) = A\cos(\xi)$. The number of iterations was chosen to be 10^3. The initial condition for velocity potential was: $\phi = c_0 A \coth(hk) \cdot \sin(X)$ with $k = 1$. We considered right-traveling waves, which correspond to the $+$ sign in (18). For such initial conditions, wave distortion would occur only due to nonlinear effects. The purpose of this work was to systematically study the system of Equations (16) and (17) for various control parameters of Ω, E_b, and h.

3.1. Deep Water, h = 10

First, we considered the case of deep water, i.e., we set the fluid depth to $h = 10$. Figure 2a shows the evolution of the free surface in the absence of vorticity and an external tangential electric field. Despite the fact that the amplitude of the surface wave was quite large $A = 0.5$, the deformations were relatively small. In general, for these parameters, the system demonstrated weakly nonlinear quasi-periodic chaotic behavior. In the case of a small wave amplitude, the weak turbulence of collinear capillary waves could develop on the surface of a deep fluid [44,45]. Figure 2b shows the calculated time dependence $D(t)$. It can be seen that the deviation of $D(t)$ from h was very small. The energy deviation from the initial value $\Delta H = H(t) - H(0)$ is shown in Figure 2c. The value of the quantity ΔH did not exceed 10^{-11}. Thus, the developed numerical setup made it possible to simulate the nonlinear dynamics of a liquid surface with high spectral accuracy.

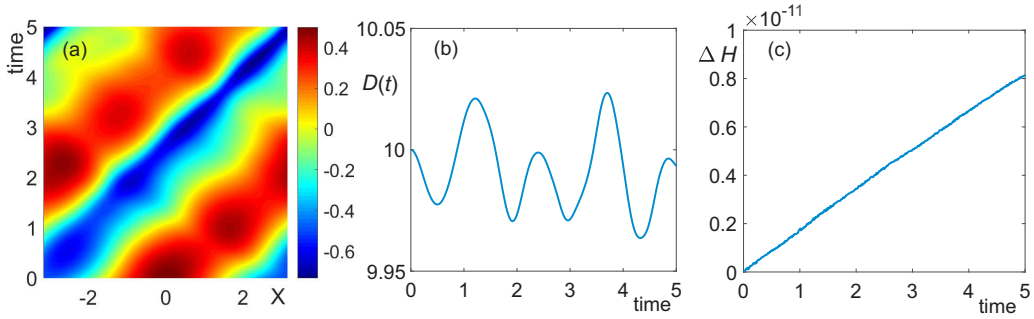


Figure 2. (**a**) The spatial–temporal evolution of the free surface for zero vorticity $\Omega = 0$, (**b**) the time dependence of the parameter $D(t)$, and (**c**) the difference in energy (15) with the initial value at each time step. The simulation parameters were $A = 0.5$, $h = 10$, and $E_b = 0$.

Figure 3 shows the dynamics of free-surface waves for positive vorticity $\Omega = 4$. From this figure, one can see that the shear flow slowed down the propagation of the wave. In this case, the wave deformation was much more noticeable than in the case of zero vorticity shown in previous figure. The effect of vorticity with negative sign $\Omega = -4$ is shown in Figure 4. In this figure, one can see two important effects: wave acceleration and the formation of large-amplitude waves. The first effect is simply explained by the linear dispersion relation (18). The formation of large-amplitude waves is a completely nonlinear effect. The figure shows that the wave amplitude increased almost twice in comparison with the initial value, $A = 0.35$.

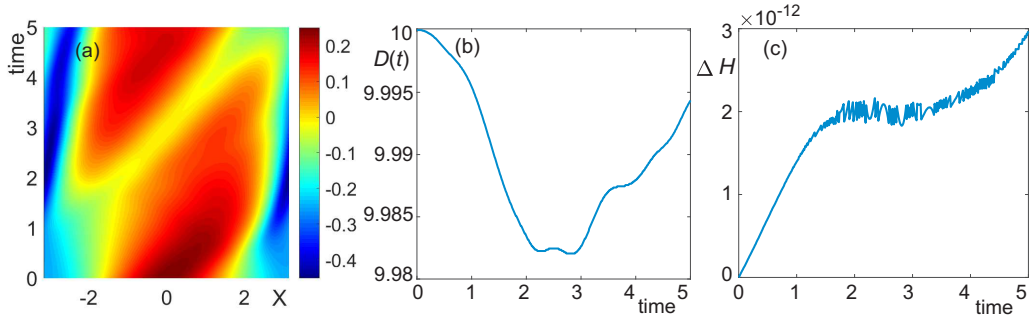


Figure 3. (**a**) The spatial–temporal evolution of the free surface for $\Omega = 4$, (**b**) the time dependence of the parameter $D(t)$, and (**c**) the difference in energy (15) with the initial value at each time step. The simulation parameters were $A = 0.25$, $h = 10$, and $E_b = 0$.

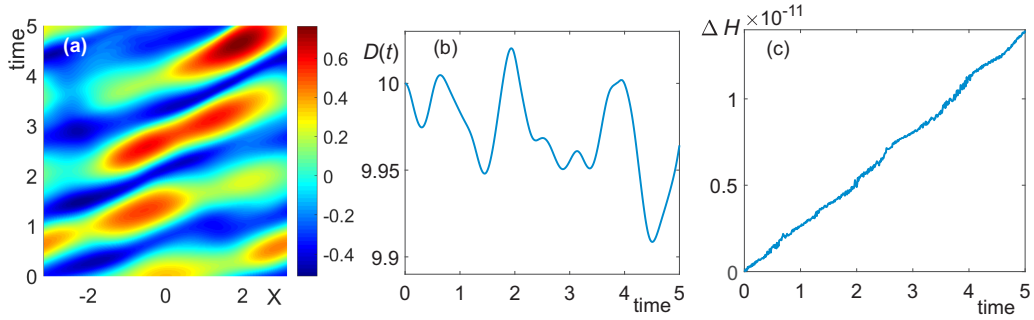


Figure 4. (**a**) The spatial–temporal evolution of the free surface for $\Omega = -4$, (**b**) the time dependence of the parameter $D(t)$, and (**c**) the difference in energy (15) with the initial value at each time step. The simulation parameters were $A = 0.35$, $h = 10$, and $E_b = 0$.

The main question of the current study is what effect a tangential electric field has on the dynamics of a fluid boundary with constant vorticity. Figure 5 shows the evolution of the free surface for a high enough electric field $E_b = 100$ and positive vorticity $\Omega = 4$, which slowed down the wave propagation. The evolution of the surface for a high field was very different from the wave dynamics for zero field, as shown in Figure 3. It can be seen that the

traveling wave retained its shape despite the presence of shear flow. Thus, with an increase in the electric field, the system entered a regular mode of motion, when the propagation of nonlinear waves occurred at a constant speed and almost without distortions. Such a regime is a complete analog of Alfvèn waves in plasmas. The interaction of waves is only possible for oppositely traveling waves [39].

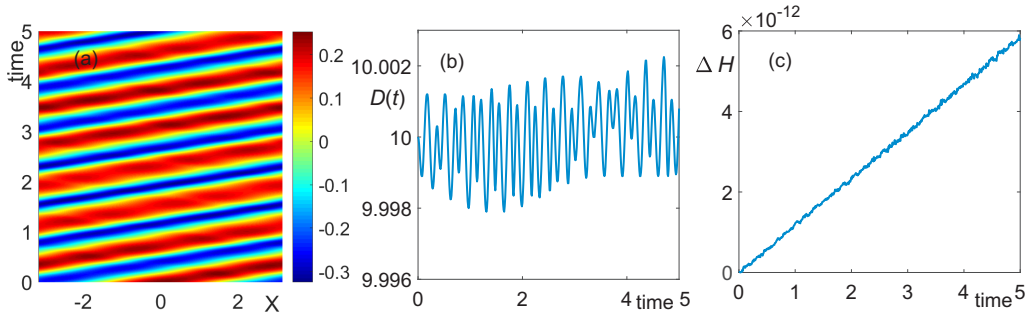


Figure 5. (**a**) The spatial–temporal evolution of the free surface for $\Omega = 4$, (**b**) the time dependence of the parameter $D(t)$, and (**c**) the difference in energy (15) with the initial value at each time step. The simulation parameters were $A = 0.25$, $h = 10$, and $E_b = 100$.

3.2. Intermediate Depth, $h = 1$

In this section, we present the simulation results for intermediate depth, $h = 1$. Figure 6a shows the spatial–temporal evolution of the free surface in the absence of vorticity and an electric field. In general, the behavior of the system at intermediate depths was very similar to the dynamics of waves on the surface of deep water shown in Figure 2a. The difference was that the parameter $D(t)$ (conformal depth) deviated more noticeably from the physical depth h (see Figure 6b). A noticeable difference was also observed in the magnitude of the computational error shown in Figure 6c. Apparently, the use of an iterative method of searching the parameter $D(t)$ reduced the accuracy of the calculations.

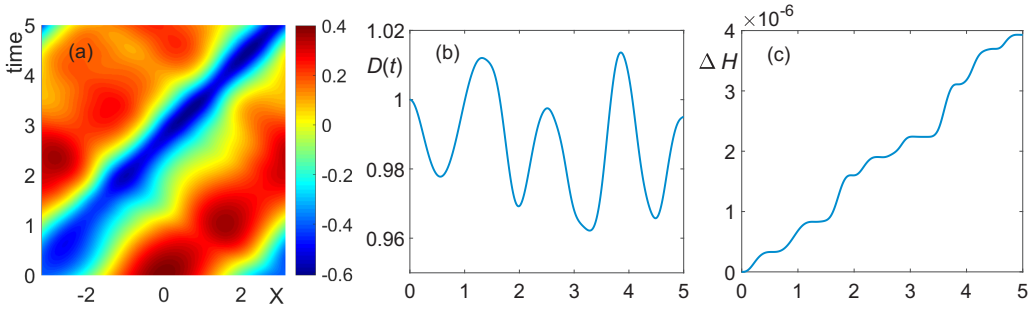


Figure 6. (**a**) The spatial–temporal evolution of the free surface for zero vorticity $\Omega = 0$, (**b**) the time dependence of the parameter $D(t)$, and (**c**) the difference in energy (15) with the initial value at each time step. The simulation parameters were $A = 0.4$, $h = 1$, and $E_b = 0$.

Figure 7a shows the dynamics of a gravity–capillary wave for strong positive vorticity $\Omega = 6$. It is clearly seen that the wave deformation was very strong despite the relatively small amplitude, $A = 0.2$. Another important feature observed in Figure 7a was that the wave propagated in the opposite direction to the linear wave. The speed of a linear wave (18) propagating to the right is positive for any value of vorticity. Thus, the effect of the retrograde motion of the surface wave under positive vorticity is a pure nonlinear effect. Figure 8 shows the evolution of the surface wave for strong negative vorticity $\Omega = -6$, which accelerated the wave propagation. One can see that the tendencies observed in Figure 4 were strengthened. The strong negative vorticity led to the formation of waves of large amplitude and an increase in their speed.

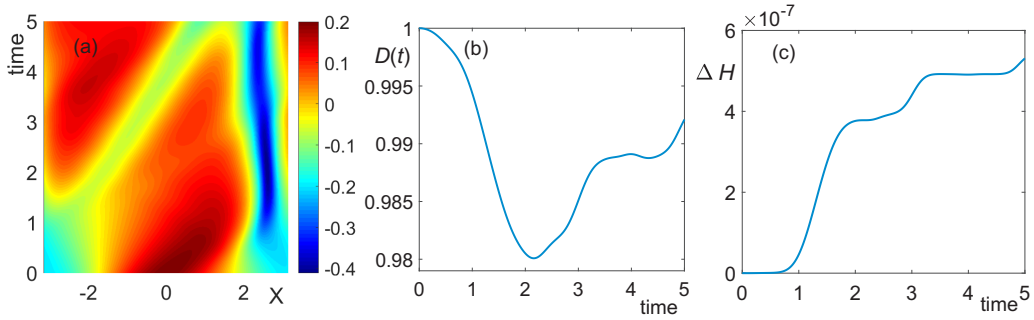


Figure 7. (**a**) The spatial–temporal evolution of the free surface for $\Omega = 6$, (**b**) the time dependence of the parameter $D(t)$, and (**c**) the difference in energy (15) with the initial value at each time step. The simulation parameters were $A = 0.2$, $h = 1$, and $E_b = 0$.

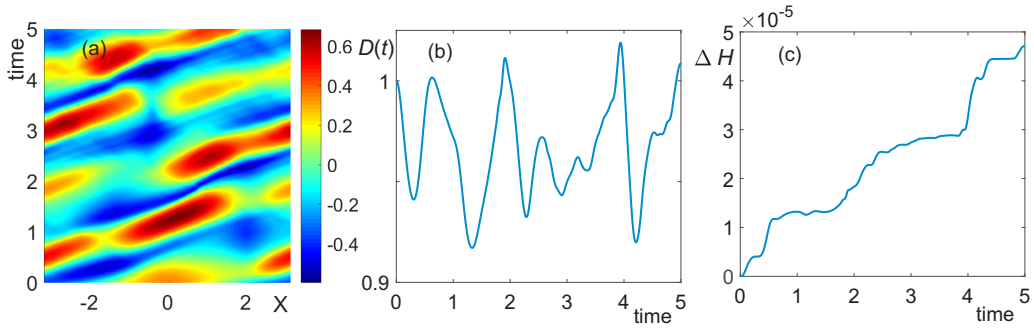


Figure 8. (**a**) The spatial–temporal evolution of the free surface for $\Omega = -6$, (**b**) the time dependence of the parameter $D(t)$, and (**c**) the difference in energy (15) with the initial value at each time step. The simulation parameters were $A = 0.35$, $h = 1$, and $E_b = 0$.

An interesting nonlinear effect appeared at the liquid boundary with a further increase in vorticity to $\Omega = -9$ (see Figure 9a). At such a large value of Ω, we observed the wave breaking process with the formation of a bubble inside the liquid (see Figure 9b). To our knowledge, this is the first numerical observation of a wave breaking due to a strong shear flow co-directed in the wave propagation direction.

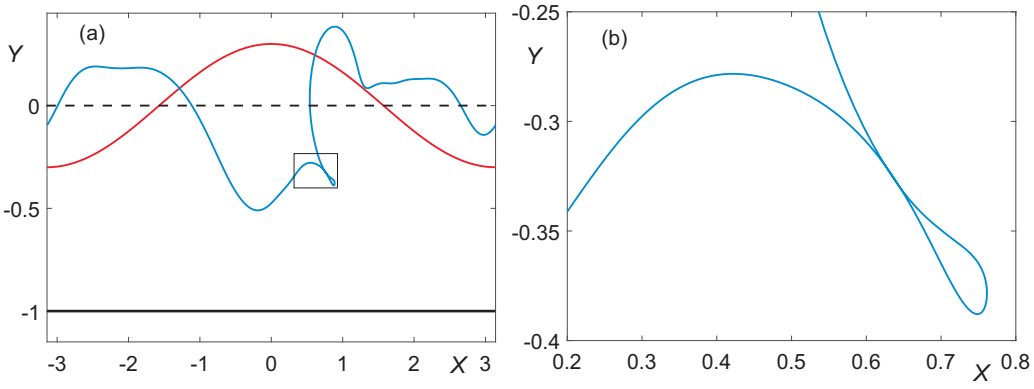


Figure 9. (**a**) The free-surface profile shown at the initial moment (red line) and at the moment of bubble formation $t \approx 1.27$ (blue line); (**b**) the surface shown at the range $X \in [0.2, 0.8]$. The simulation parameters were $\Omega = -9$, $A = 0.3$, $h = 1$, and $E_b = 0$.

At the end of this section, we show the dynamics of the free surface for a strong tangential electric field (see Figure 10). The initial conditions for this figure were the same as in Figure 7. It can be seen that for an intermediate depth, the system entered the electro-hydrodynamic regime of motion, for which the wave deformation was very small.

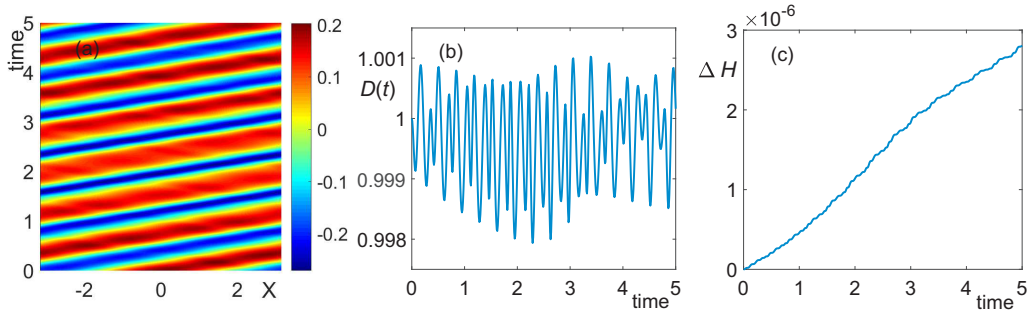


Figure 10. (**a**) The spatial–temporal evolution of the free surface for $\Omega = 6$, (**b**) the time dependence of the parameter $D(t)$, and (**c**) the difference in energy (15) with the initial value at each time step. The simulation parameters were $A = 0.2$, $h = 1$, and $E_b = 100$.

3.3. Shallow Water, $h = 0.1$

The wave dynamics for the shallow water case are presented in this section. The physical depth was assumed to be $h = 0.1$. The dynamics of a gravity–capillary wave in the absence of a field and vorticity are shown in Figure 11. One can see that the speed of wave propagation in shallow water was much lower than in deep water, as shown in Figure 2. As the fluid depth decreased, the effect of shear flow weakened for a fixed value of Ω. For this reason, we considered the motion of waves with a very high vorticity of $\Omega = 8$ (see Figure 12). It can be seen that the previously observed trends for waves with positive vorticity remained the same for the case of shallow water. The shear flow directed against the propagation of the wave slowed it down.

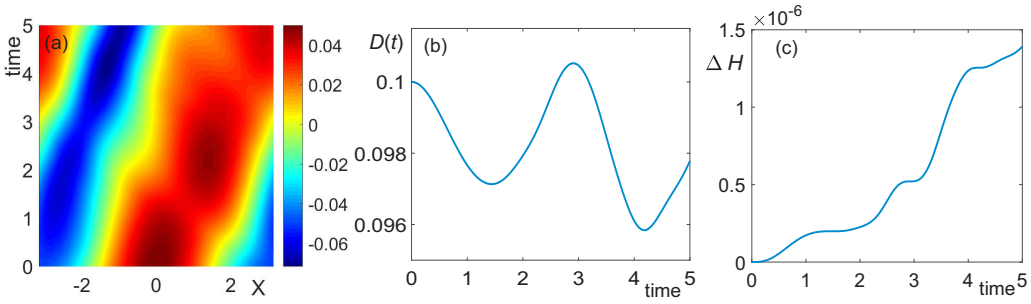


Figure 11. (**a**) The spatial–temporal evolution of the free surface for zero vorticity $\Omega = 0$, (**b**) the time dependence of the parameter $D(t)$, and (**c**) the difference in energy (15) with the initial value at each time step. The simulation parameters were $A = 0.05$, $h = 0.1$, and $E_b = 0$.

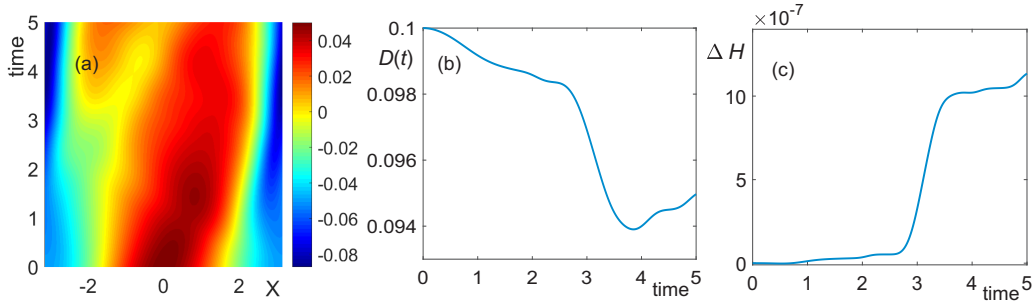


Figure 12. (**a**) The spatial–temporal evolution of the free surface for $\Omega = 8$, (**b**) the time dependence of the parameter $D(t)$, and (**c**) the difference in energy (15) with the initial value at each time step. The simulation parameters were $A = 0.05$, $h = 0.1$, and $E_b = 0$.

The evolution of a surface wave with negative vorticity is shown in Figure 13. Due to the weak influence of vorticity at shallow depths, we did not observe the formation of strongly nonlinear waves with a large amplitude as in Figures 4 and 8. Figure 13 shows only a slight increase in the wave speed. The deformations were as weak as for the case of

zero vorticity (see Figure 11). The electro-hydrodynamic regime of fluid motion is shown in Figure 14. It can be seen that the regime of wave propagation without distortions could also be realized for the case of shallow water.

Finally, we note that the accuracy of the calculations remained high for all calculation parameters. The computational error for all numerical experiments did not exceed a small value of the order 10^{-6}. Note also that the simulation results were in very good agreement with Zubarev's exact analytical solution obtained for the case of a strong horizontal electric field (see [7,8]). Thus, the obtained results demonstrated high accuracy and reliability.

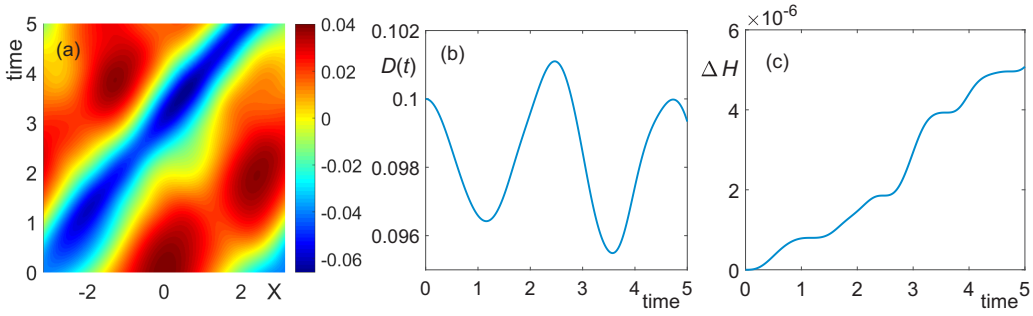


Figure 13. (**a**) The spatial–temporal evolution of the free surface for $\Omega = -8$, (**b**) the time dependence of the parameter $D(t)$, and (**c**) the difference in energy (15) with the initial value at each time step. The simulation parameters were $A = 0.04$, $h = 0.1$, and $E_b = 0$.

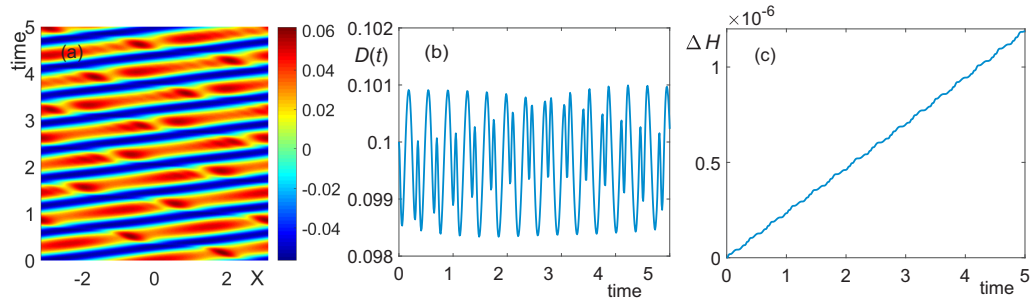


Figure 14. (**a**) The spatial–temporal evolution of the free surface for $\Omega = 8$, (**b**) the time dependence of the parameter $D(t)$, and (**c**) the difference in energy (15) with the initial value at each time step. The simulation parameters were $A = 0.05$, $h = 0.1$, and $E_b = 100$.

4. Conclusions

The nonlinear dynamics of the free surface of a finite-depth fluid with linear shear flow was studied numerically in the current work. The numerical method used in the work was based on the time-dependent conformal transformation of the region occupied by the liquid into a strip of canonical variables. The combined effects of a horizontal electric field and linear shear flow were taken into account for the first time. A systematic study of the nonlinear dynamics of the fluid surface for a wide range of control parameters (depth, vorticity, and electric field) was carried out in this work. In the regime of high vorticity and zero external field, the system demonstrated quite complicated nonlinear behavior. In the case of a co-directional shear flow to the wave propagation direction, the process of wave breaking with the formation of an air bubble inside the fluid was observed for the first time. For an oppositely directed shear flow, the retrograde motion of the wave was observed when its propagation occurred against the speed of the linear wave. Both processes are fully nonlinear, and their theoretical description requires further intensive studies. The included horizontal electric field prevented the development of these processes: the free-surface waves tended to preserve their shape. Thus, under a strong horizontal electric field, the system could enter the pure electro-hydrodynamic regime of motion, which is an analog of Alfvèn wave propagation in conducting media or plasmas.

Author Contributions: M.V.F.: conceptualization, investigation, methodology, writing (original draft), and writing (review and editing). R.R.-J.: conceptualization, investigation, methodology, writing (original draft), and writing (review and editing). E.K.: conceptualization, investigation, methodology, writing (original draft), and writing (review and editing). All authors have read and agreed to the published version of the manuscript.

Funding: Section 3 of this work was supported by the Russian Science Foundation, project No. 23-71-10012 .

Data Availability Statement: Data sharing is not applicable to this article as no new data were created or analyzed in this study.

Acknowledgments: The work of E. Kochurin in Section 3 was supported by the Russian Science Foundation, project No. 23-71-10012. The authors M.V.F. and R.R.-J. are grateful to IMPA for hosting them as visitors during the 2023 Post-Doctoral Summer Program.

Conflicts of Interest: The authors declare no conflict of interest.

References

1. Papageorgiou, D.T. Film flows in the presence of electric fields. *Annu. Rev. Fluid Mech.* **2019**, *51*, 155–187. [CrossRef]
2. Melcher, J.R. Electrohydrodynamic and magnetohydrodynamic surface waves and instabilities. *Phys. Fluids* **1961**, *4*, 1348. [CrossRef]
3. Guo, W.; Zhang, Q.; He, D. On the nonlinear behaviour of the Rayleigh–Taylor instability with a tangential electric field for inviscid and perfect dielectric fluids. *J. Fluid Mech.* **2023**, *958*, A36. [CrossRef]
4. Deng, X.D.; Wang, P.; Shi, B.L.; Fu, Q.F.; Jia, B.Q. Temporal instability of a viscous liquid film on an oscillating plane in the presence of static electric field. *AIP Adv.* **2023**, *13*, 045019. [CrossRef]
5. Zhilenko, D.Y.; Krivonosova, O.E. Suppression of the instability of rotating flows. *Tech. Phys. Lett.* **2022**, *48*, 156–160. [CrossRef]
6. Li, D.; Li, Y.; Li, Z.; Wang, Y. Theory analyses and applications of magnetic fluids in sealing. *Friction* **2023**, *11*, 1771–1793. [CrossRef]
7. Zubarev, N.M. Nonlinear waves on the surface of a dielectric liquid in a strong tangential electric field. *Phys. Lett. A* **2004**, *333*, 284–288. [CrossRef]
8. Zubarev, N.M. Nonlinear waves on the surface of a dielectric liquid in a horizontal electric field in 3D geometry: Exact solutions. *JETP Lett.* **2009**, *89*, 271–274. [CrossRef]
9. Zubarev, N.M. Formation of root singularities on the free surface of a conducting fluid in an electric field. *Phys. Lett. A* **1998**, *243*, 128–131. [CrossRef]
10. Zubarev, N.M. Exact solutions of the equations of motion of liquid helium with a charged free surface. *J. Exp. Theor. Phys.* **2002**, *94*, 534–554. [CrossRef]
11. Galtier, S. Turbulence in space plasmas and beyond. *J. Phys. A Math. Theor.* **2018**, *51*, 293001. [CrossRef]
12. Boyer F; Falcon, E. Wave turbulence on the surface of a ferrofluid in a magnetic field. *Phys. Rev. Lett.* **2008**, *101*, 244502. [CrossRef]
13. Dorbolo, S.; Falcon, E. Wave turbulence on the surface of a ferrofluid in a horizontal magnetic field. *Phys. Rev. E* **2011**, *83*, 046303. [CrossRef]
14. Ricard, G.; Falcon, E. Transition from wave turbulence to acousticlike shock-wave regime. *Phys. Rev. Fluids* **2023**, *8*, 014804. [CrossRef]
15. Kochurin, E.A. Wave turbulence of a liquid surface in an external tangential electric field. *JETP Lett.* **2019**, *109*, 303–308. [CrossRef]
16. Kochurin, E.; Ricard, G.; Zubarev, N.; Falcon, E. Three-dimensional direct numerical simulation of free-surface magnetohydrodynamic wave turbulence. *Phys. Rev. E* **2022**, *105*, L063101. [CrossRef] [PubMed]
17. Dmitriev, I.A.; Kochurin, E.A.; Zubarev, N.M. Numerical study of free-surface electro-hydrodynamic wave turbulence. *IEEE Trans. Dielectr. Electr. Insul.* **2023**, *30*, 1408–1413. [CrossRef]
18. Crapper, G.D. An exact solution for progressive capillary waves of arbitrary amplitude. *J. Fluid Mech.* **1957**, *2*, 532–540. [CrossRef]
19. Longuet-Higgins, M.S. The instabilities of gravity waves of finite amplitude in deep water I. Superharmonics. *Proc. R. Soc. Lond.* **1978**, *360*, 471–488. [CrossRef]
20. Tiron, R.; Choi, W. Linear stability of finite-amplitude capillary waves on water of infinite depth. *J. Fluid Mech.* **2012**, *696*, 402–422. [CrossRef]
21. Vanden-Broeck, J.-M. New families of steep solitary in water of finite depth with constant vorticity. *Eur. J. Mech. B Fluids* **1995**, *14*, 761–774.
22. Choi, W. Nonlinear surface waves interacting with a linear shear current. *Math. Comput. Simul.* **2009**, *80*, 29–36. [CrossRef]
23. Gao, T.; Milewski, P.A.; Wang, Z. Capillary-gravity solitary waves on water of finite depth interacting with a linear shear current. *Stud. Appl. Math.* **2021**, *147*, 1036–1057. [CrossRef]
24. Murashige, S.; Choi, W. Parasitic Capillary Waves on Small-Amplitude Gravity Waves with a Linear Shear Current. *J. Mar. Sci. Eng.* **2021**, *9*, 1217. [CrossRef]
25. Hur, V.M.; Wheeler, M.H. Exact free surfaces in constant vorticity flows. *J. Fluid Mech.* **2020**, *896*, R1. [CrossRef]
26. Lokharu, E. On the amplitude and the flow force constant of steady water waves. *J. Fluid Mech.* **2021**, *921*, A2. [CrossRef]

27. Lokharu, E.; Wahlèn, E.; Weber, J. On the Amplitude of Steady Water Waves with Favorable Constant Vorticity. *J. Math. Fluid. Mech.* **2023**, *25*, 58. [CrossRef]
28. Hunt, M.J.; Dutykh, D. Free surface flows in electrohydrodynamics with a constant vorticity distribution. *Water Waves* **2021** , *3*, 297–317. [CrossRef]
29. Flamarion, M.V.; Gao, T.; Ribeiro-Jr, R.; Doak, A. Flow structure beneath periodic waves with constant vorticity under normal electric fields. *Phys. Fluids* **2022**, *34*, 127119. [CrossRef]
30. Ovsjannikov, L.V. To the shallow water theory foundation. *Arch. Mech.* **1974**, *26*, 6.
31. Dyachenko, A.I.; Kuznetsov, E.A.; Spector, M.; Zakharov, V.E. Analytical description of the free surface dynamics of an ideal fluid (canonical formalism and conformal mapping). *Phys. Lett. A* **1996**, *221*, 736. [CrossRef]
32. Zakharov, V.E.; Dyachenko, A.I.; Vasilyev, O.A. New method for numerical simulation of a nonstationary potential flow of incompressible fluid with a free surface. *Eur. J. Mech. B Fluids* **2002**, *21*, 283. [CrossRef]
33. Ruban, V.P. Waves over curved bottom: The method of composite conformal mapping. *J. Exp. Theor. Phys.* **2020**, *130* 797–808. [CrossRef]
34. Ruban, V.P. Water waves over a time-dependent bottom: Exact description for 2D potential flows. *Phys. Lett. A* **2005**, *340*, 194–200. [CrossRef]
35. Korotkevich, A.O.; Prokofiev, A.; Zakharov, V.E. On the dissipation rate of ocean waves due to white capping. *JETP Lett.* **2019**, *109*, 309–315. [CrossRef]
36. Dyachenko, S.; Newell, A.C. Whitecapping. *Stud. Appl. Math.* **2016**, *137*, 199–213. [CrossRef]
37. Nachbin, A. Water wave models using conformal coordinates. *Physica D* **2023**, *445*, 133646. [CrossRef]
38. Dyachenko, S.A.; Semenova, A. Canonical conformal variables based method for stability of Stokes waves. *Stud. Appl. Math.* **2023**, *150*, 705–715. [CrossRef]
39. Kochurin, E.A. Formation of regions with high energy and pressure gradients at the free surface of liquid dielectric in a tangential electric field. *J. Appl. Mech. Tech. Phys.* **2018**, *59*, 79–85. [CrossRef]
40. Gao, T.; Milewski, P.A.; Papageorgiou, D.T.; Vanden-Broeck, J.M. Dynamics of fully nonlinear capillary–gravity solitary waves under normal electric fields. *J. Eng. Math.* **2018**, *108*, 107–122. [CrossRef]
41. Gao, T.; Doak, A.; Vanden-Broeck, J.M.; Wang, Z. Capillary–gravity waves on a dielectric fluid of finite depth under normal electric field. *Eur. J. Mech. B Fluids* **2019**, *77*, 98–107. [CrossRef]
42. Gao, T.; Wang, Z.; Vanden-Broeck, J.M. Nonlinear wave interactions on the surface of a conducting fluid under vertical electric fields. *Phyica D* **2023**, *446*, 133651. [CrossRef]
43. Doak, A.; Gao, T.; Vanden-Broeck, J.M. Global bifurcation of capillary-gravity dark solitary waves on the surface of a conducting fluid under normal electric fields. *Q. J. Mech. Appl. Math.* **2022**, *75*, 215–234. [CrossRef]
44. Kochurin, E.; Ricard, G.; Zubarev, N.; Falcon, E. Numerical simulation of collinear capillary-wave turbulence. *JETP Lett.* **2020**, *112*, 757–763. [CrossRef]
45. Ricard, G.; Falcon, E. Experimental quasi-1D capillary-wave turbulence. *Europhys. Lett.* **2021**, *135*, 64001. [CrossRef]

Disclaimer/Publisher's Note: The statements, opinions and data contained in all publications are solely those of the individual author(s) and contributor(s) and not of MDPI and/or the editor(s). MDPI and/or the editor(s) disclaim responsibility for any injury to people or property resulting from any ideas, methods, instructions or products referred to in the content.